First-principles calculations of iodine-related point defects in $CsPbI_3$

R. A. Evarestov[*a], *A. Senocrate*[b,c], *E. A. Kotomin*[b,d], *J.Maier*[b]

[a] Institute of Chemistry, St.Petersburg State University, Petrodvorets, Russia, E-mail: r.evarestov@spbu.ru

[b] Max Planck Institute for Solid State Research , Stuttgart, Germany

[c] École Polytechnique Fédérale de Lausanne, Switzerland

[d] Institute of Solid State Physics, University of Latvia, Riga, Latvia

Abstract

We present here first principles hybrid functional calculations of the atomic and electronic structure of several iodine-related point defects in $CsPbI_3$, a material relevant for photovoltaic applications. We show that the presence of neutral interstitial I atoms or electron holes leads to the formation of di-halide dumbbells I_2^- (analogously to the well-known situation in alkali halides). Their formation and one-electron energies in the band gap are determined. The formation energy of the Frenkel defect pair (I vacancy and neutral I interstitial) is found to be ~1 eV, and as such smaller than the band gap. We conclude that both iodine dumbbells and iodine vacancies could be, in principle, easily produced by interband optical excitation.

Introduction

Halide perovskites have recently found themselves in the spotlight due to their remarkable photo-electrochemical properties and their potential to be used as highly efficient, solution-processable light harvesters for photovoltaic devices.[1] Among these materials, iodine-based formulations have shown the highest promise; in particular, the organic-inorganic methylammonium lead triiodide ($CH_3NH_3PbI_3$) has been extensively studied. Despite its outstanding functional properties, this material (and in general the hybrid formulations) suffers from major shortcomings, in particular from high instability, which can be largely attributed to the presence of the organic cation. Searching for alternatives, the fully inorganic $CsPbI_3$ fulfill most criteria, and while its photo-electrochemical properties still fall short of its hybrid

counterpart, its high stability is very attractive for practical application. Interestingly, performances of $CsPbI_3$-based photovoltaic devices have increased significantly[2,3] since their first report.[4]

In this study, we investigate point defect formation and basic properties in $CsPbI_3$ from first principles calculations. Despite being of great importance, a thorough investigation of point defects in this material is still very limited.[5,6] Indeed, many halide perovskites (including $CsPbI_3$) are already known to be mixed ionic-electronic conductors,[7–10] and as such investigating ionic defect formation (and migration) provides important information on their charge transport properties. The presence of point defects is also expected to influence the electronic transport (and device performance) in these materials, both considering mobile defects (coupling of ionic and electronic transport, interfacial redistribution phenomena) and static ones (electronic carriers trapping and recombination processes).

Based on the previous knowledge on $CH_3NH_3PbI_3$, we study iodine-related defects, which have been shown extensively to be the most mobile (and likely the highest in concentration) both experimentally[11,12] and computationally.[13–17] Note that substantial iodine migration has been experimentally observed in $CsPbI_3$ as well.[7] In particular, we focus here on hole and electron trapping by iodine defects, which is receiving an increasing attention[18–22] in halide perovskites, due to its relation to recombination processes and potentially to the remarkable photo-enhancement of ionic transport.[23] Previous studies[18–20] suggest favorable formation of iodine dumbbells (I_2^- aggregates within the crystal structure) by trapping of electron holes, but mechanistic insights are largely lacking. Here, we show that these aggregates also are expected to form in $CsPbI_3$. By performing first principles calculation without *a priori* assumption on the formation process, we will also unveil the mechanism of generation of these extended defects.

Halide-related defects are well studied in alkaline-earth halides (e.g. CaF_2, MgF_2), alkali halides MeX (e.g. KCl), including iodides (e.g. KI, NaI, RbI).[24–29] It is well established that in these materials interband optical excitations (light or UV) create excess electrons and electron holes.

The self-trapping of electron holes on halide sites leads to the formation of dimers X_2^- called the V_k centers (association of a neutralized halide with a X^-, both initially on regular lattice sites).[30] Recombination of electrons with V_k centers leads to the formation of self-trapped excitons, whose non-radiative decay, in turn, results in the formation of neutral Frenkel defect pairs, i.e. halide vacancies with trapped electrons (the *F* center) and interstitial halide atoms with trapped electron holes. The latter is chemically unstable with respect to the formation of the X_2^- dumbbell (the *H* center) upon involvement of another regular lattice halide. The difference between the H and V_k centers is that the former occupies a single halide site and thus is a neutral defect with respect to the perfect crystalline lattice whereas the V_k center has a slightly longer bond length and partially occupies two lattice sites (and thus is effectively positively charged). Interaction of these primary defects with each other or with intrinsic, pre-radiation defects can lead to the formation of even more complex defects, e.g. trimers X_3^{2-}. [31] Formation of radiation (light)-induced interstitial dumbbells was discussed also in binary oxides such as MgO,[32,33] SrO [34] and Al_2O_3.[35,36]

Methods

Our first-principles periodic calculations were performed in the frame of the hybrid DFT PBESOL0 implemented in the CRYSTAL17 code[37]. This is a hybrid version of PBE exchange-correlation (XC) functional with 25% of Hartree-Fock exchange and revised for solids PBESOL[38] XC functional instead of PBE XC functional. Gaussian atomic orbitals[39] were used to expand the crystalline Bloch functions. The interaction between the core electrons and the valence and sub-valent electrons in iodine, lead and cesium atoms and the valence electrons was described by means of the effective core pseudopotentials. For sodium atoms, an all-electron basis set[38] was used. The reciprocal-space Brillouin zone (BZ) sampling was performed with 8x8x8 **k**-point meshes generated according to the Monkhorst Pack scheme.[40] Kohn-Sham equations were solved iteratively to self-consistency within 10^{-8} eV. Full geometry optimization was carried out both in perfect and defective crystals calculations. The Mulliken analysis was used for effective atomic charges.

In the point defects calculations, the supercell model[41] with a 2x2x2 supercell was used. In the perfect cubic $CsPbI_3$ crystal, three Wyckoff positions of the space group Pm-3m with the simple cubic lattice are occupied: Cs 1b (0.5,0.5,0.5), Pb 1a (0,0,0), I 3d (0.5,0,0). The H-center

was modelled by introducing a neutral iodine atom in the interstitial *c*- position with the coordinates (0.25,0.25,0) in the supercell. The V_k center was modeled by substitution of a Pb atom by a Na atom, in order to imitate the presence of an electron hole within the supercell (acceptor doping). Its localization was calculated during self-consistent atomic and electronic structure relaxation to the minimum of total energy, without any *a priori* assumptions. The *F*-center was modelled by creating a neutral iodine vacancy in the supercell. In the correlated Frenkel pair calculations the distance between defects was 6.3 Å. The energy of this well-separated pair was calculated as a sum of the formation energies for the *H* and *F* centers. In defect calculations, both atomic positions and the lattice parameters were optimized to get the minimum of the total energy of the supercell. The initial cubic structure was considerably distorted by the creation the defects.

To estimate the point defect formation energies (E_f) for the *H* center, the sum of the perfect crystal supercell E_{perf} and the chemical potential U_I of iodine was subtracted from the total energy E_{def} of the defective crystal supercell (Eq. 1). For the V_k center, we use charge correction by including the difference between lead and sodium chemical potentials U_{Pb}, U_{Na} (Eq. 2). For the *F* center, iodine chemical potential U_I was subtracted from E_{perf} (Eq. 3). The defect formation energies E_f were calculated using the following relations:

H center: $E_f = E_{def} - (E_{perf} + U_I)$ (1)

V_k center: $E_f = E_{def} - (E_{perf} + U_{Pb} - U_{Na})$ (2)

F center: $E_f = E_{def} - (E_{perf} - U_I)$ (3)

Frenkel pair: $E_f = E_{def} - E_{perf}$ (4)

The chemical potentials U_I, U_{Pb}, U_{Na} were found by calculating (with geometry optimization) the total energies of a free I_2 molecule, and of PbI_2 and NaI crystals respectively. The relaxation energies (volume change) were calculated as the difference of total energies (supercell volumes) before and after geometry optimization.

Results

Table 1 shows that the chosen functional allows us to well reproduce both the atomic structure and band gap of three related materials $CsPbX_3$ (X=Cl, Br, I). The calculated lattice constants deviate from experimental ones less than 1 %. The spin-orbital interactions were neglected in our calculations. It was shown[18] that their inclusion leads to the increase of the valence band top by 0.2 eV and to the decrease of the Pb-based conduction band bottom by 0.8 eV. Taking this correction into account, our calculations in good agreement with experimental band gaps.

Table 1. Calculated basic properties of the perfect crystals. a_0 cubic lattice constant (Å), E_g band gap (eV), SO-spin-orbit interaction, q effective atomic charges (e).

	a_0 (expt)	**a_0 (calc)**	**E_g (expt)**	**E_g (calc without SO)**	**Eg (calc. incl. SO)**	**q (Cs)**	**q (Pb)**	**q(X)**
$CsPbCl_3$	5.60[42]	5.68	3.0[43]	3.9	2.9	0.99	1.18	-0.73
$CsPbBr_3$	5.87[42]	5.94	2.4[43]	3.1	2.1	0.99	0.95	-0.65
$CsPbI_3$	6.29[44]	6.33	1.7[43]	2.7	1.7	0.99	0.85	-0.62

Considering the effective ionic charges, Cs ions are always close to +1e, while halide charges are smaller than -1e due to the Pb-X bond covalency. As expected, covalency effects appears larger for iodides. The calculated bond lengths of neutral X_2 molecules and X_2^- ions (important for the *H* and V_k centers) are in a good agreement with experimental values for all considered halides (Table 2), with only a small deviation from experimental values of 4-5 %.

Table 2. Bond lengths (Å) and chemical potentials (atomic units) of halides.

X	**R_{X-X} (X_2) Expt**	**R_{X-X} (X_2) calc.**	**U_X calc.**	**R_{X-X} (X_2^-) expt**	**R_{X-X} (X_2^-) calc.**
Cl	1.99[45]	2.18	-14.867218	2.62[45]	2.74
Br	2.28[45]	2.41	-13.333277	2.85[45]	2.96
I	2.67[45]	2.84	-11.388158	3.23[45]	3.35

Fig. 1 shows the starting and optimized atomic structures of the *H* and V_k centers in $CsPbI_3$. Introducing a single interstitial I atom directly leads to the formation of an I dumbbell through the interaction of an interstitial atom with a neighboring host I^- ion. This process is accompanied

by a considerable distortion of the lattice surrounding the defect, not only locally but also at long range. This is confirmed by the analysis of the initially cubic crystalline structure upon formation of the *H* center (Table 3). All lattice parameters distort and cease to be equivalent, while the angles between them in the triclinic crystal deviate from 90º (as indicated by the parameter Δ, Table 3).

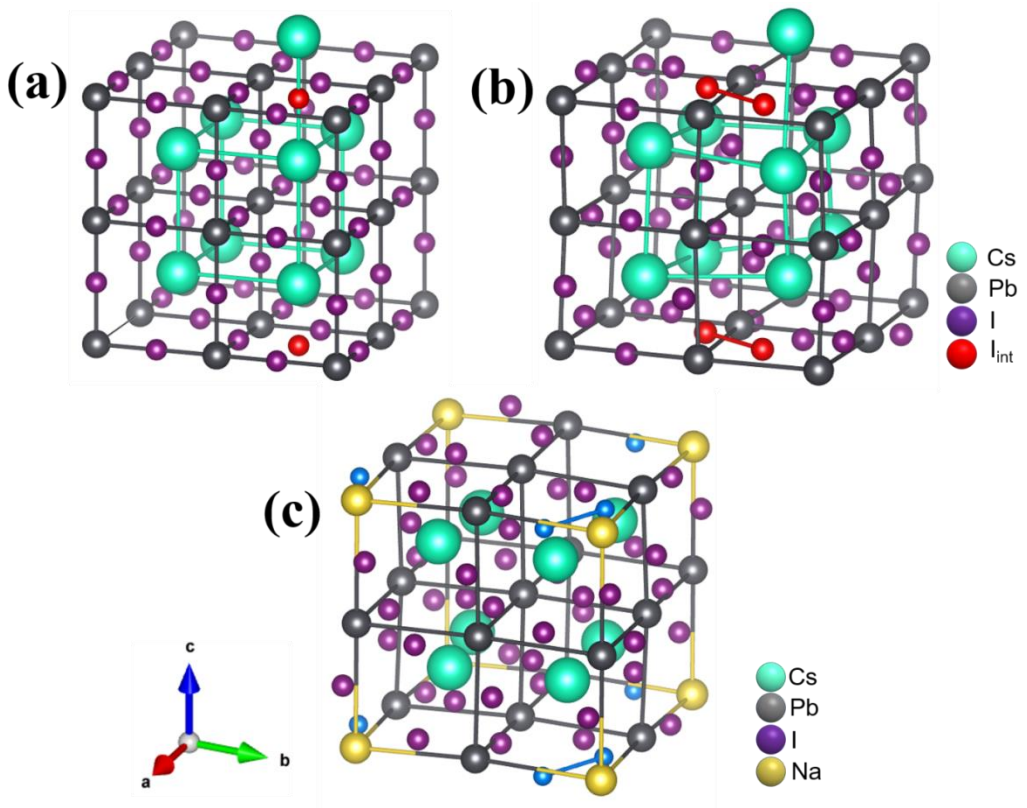

Figure 1. *H*-center formation in $CsPbI_3$. Structure before **(a)** and after **(b)** the geometry optimization. Note the additional neutral iodine inserted into an interstitial position (in red), which later interacts with a regular lattice iodine in forming the dumbbell (I-I bond, red). Notice the considerable lattice distortion deriving from the inclusion of the defect. **(c)** V_K-center formation in $CsPbI_3$ upon addition of Na dopant on Pb sites. After geometry optimization, a dumbbell forms, indicated by an I-I bond (blue).

We note that the *H* center formation is energetically favorable (E_f = -0.37 eV), notwithstanding the inclusion of the interstitial I atom. The dumbbell formation is accompanied by a considerable lattice relaxation (3.64 eV). The bond distance in the dumbbell (3.32 Å) is close to that in a free I_2^- ion (3.35 Å), as also observed for the *H* centers in alkali halides.[24,25] The distance between

interstitial I atom in the dumbbell and next nearest host I ions (3.83 Å) is much larger than within the dumbbell. The dumbbell formation also causes a charge redistribution which leaves an almost identical charge on the two constituting I atoms (-0.35e, -0.42e, with a small difference due to lattice distortion from a cubic one). The charges of the surrounding I ions (Table 3) are practically unvaried with respect to the perfect crystal (-0.62 e). Interestingly, our calculations show that the formation of the trimer I_3^{2-} is also possible, but energetically less favorable by 0.62 eV.

Table 3. *H* center properties calculated in the 40 atom supercell without symmetry. E_{rel} is atomic relaxation energy (eV), E_f defect formation energy (according to eq. 1), R distance between introduced interstitial H_i atom and two nearest neighbors I_1, I_2 (Å), q atomic charges (e), Δ is the deviation from the perfect cubic crystal.

Properties	**Relaxed**	Δ
a_0,b_0,c_0, Å	12.630, 12.703, 12.595	-0.030, 0.043, -0.065
Angles, grad	90.09, 89.76, 89.01	0.09, -0.024, -0.99
E_{rel}, eV	3.64	
E_f, eV	-0.37	
R, Å	3.324, 3.828	0.159, 0.663
q(H_i,I_1,I_2)	-0.35, -0.42, -0.61	-0.35,0.20,0.01

Calculations for the V_k center (Table 4 and Fig.1,c) were performed for the symmetry σ_h and without any symmetry (C1). For both cases, a considerable lattice relaxation and a high relaxation energy were found, but unlike the *H* center, the V_k center formation energy is slightly positive (0.1 - 0.17 eV). The main difference with the *H* center is that its bond length is now considerably larger (3.39 Å), also in agreement with observations in alkali halides.[24,25] In both *H* and V_k centers, the total dumbbell charge is close to -1e, in agreement with the model formula I_2^-.

Table 4. V_k center properties. Symbols are the same as in Table 3, with the exception of E_f that represents defect formation energy as given in eq. 2.

	σ_h symmetry	**C_1 symmetry**	Δ

a,b,c, A	12.359, 12.386, 12.904	12.652, 12.483, 12.532	0.293, 0.097, 0.372
E_{rel}, eV	3.80	3.83	
E_f, eV	0.17	0.10	
R, A	3.395, 4.440	3.389, 4.521	0.224, 1.356
q (H_i, I1, I2)	-0.42, -0.46, -0.59	-0.43, -0.44, -0.73	

The formation energy of the *F* centers (Table 5) is the largest (3.1 eV) among considered defects (but still considerably smaller than typical values for the *F* centers in alkali halides)[25]. The nearest Pb ions relax by moving towards vacancy (by 0.1 - 0.2 Å). Charge analysis of surrounding ions shows that nearly one electron is localized within two ionic spheres surrounding the vacancy (2 Pb and 8 I ions), in general agreement with the *F* center model commonly used in alkali halides.

Lastly, calculations of the Frenkel pair of the close *F* and *H* centers (Table 5) indicate quite low formation energy of 0.84 eV for the couple, which is significantly smaller than the band gap. This suggests that, energetically, it could be possible for such defects to be produced by light adsorption. This mechanism was also proposed for several materials, including alkali halides,[26,28,29,31] and more recently as the cause for the remarkable photo-induced ion conduction enhancement observed for $CH_3NH_3PbI_3$.

Table 5. Calculated properties of the *F* center and Frenkel pair in $CsPbI_3$ (eqs. 3 and 4). R in the *F* center represents the distances (in Å, after structure relaxation) between nearest and next nearest I ions around vacancy, whereas in the Frenkel pair represents the distance between the interstitial H_i atom and two nearest I ions. Δ is the relevant atomic displacements (positive values mean inwards vacancy).

	***F* center**	**Close Frenkel pair**
a_0, b_0, c_0, Å	12.432, 12.548, 12.785	12.618, 12.685, 12.601
Angles, grad.	90.78, 90.02, 90.21	89.73, 91.09, 89.59
E_{form}, eV	3.08	0.84
R, Å	4.275, 4.336	3.815, 4.004
Δ, Å	0.202, 0.141	0.650, 0.839
Δq, e	-0.34 e (8 nearest I ions) -0.32 e (2 nearest Pb ions)	-0.62(H_i), -0.53, -0.64

The energy of the well-separated Frenkel defects is considerably larger (a sum of the individual defect energies for the *F* and *H* centers yields 2.7 eV). All defects produce a negative volume change (Table 6), which is a rather unexpected effect but it was observed earlier in several materials such as silicon.[46]. We note that, in the V_k center calculations, the effects of Na substitution likely contribute significantly to the negative volume change, and as such a conclusion on the volume effect caused by the self-trapped electron hole is not possible.

Table 6. Defect-induced volume changes with respect to the 40 atom supercell of a perfect crystal. Iodine defect concentrations are ~4 %, corresponding to 1 defect/supercell (24 iodine atoms). The volume change of a V_k center includes the effects caused by Na substituting Pb.

Defects	**Volume change (%)**
F	-1.7
H	-0.4
V_k	-2.3
Frenkel (close)	-0.5

Considering the potential importance that this material has for photovoltaic and optoelectronic applications, we found it of relevance to calculate the energy levels of the various defects here presented. Analysis of the defect energy levels induced in the band gap (Fig. 2) shows that the *F* center serves as a shallow donor (in agreement with other reports on $CsPbI_3$[5,6] and similar to the oxygen vacancy case in oxide perovskites[26,47]) in turn, the V_k center is a shallow acceptor. In contrast, the energy level of the *H* center lies in the middle of the band gap. Thus, this defect could trap both electrons and holes and could considerably affect the processes in photovoltaic devices.

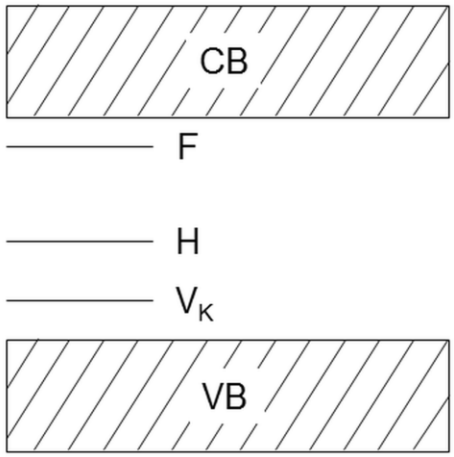

Figure 2. Schematic position of defect energy levels in the $CsPbI_3$ band gap corrected for the spin- orbital interactions. The defect energy positions relative to the top of perfect crystal valence band are 0.2 eV (V_k), 0.7 eV (H), 1.6 eV (F).

Conclusions

Our first principles supercell calculations on $CsPbI_3$ show that the interstitial I atoms tends to form an I_2^- dumbbell configuration, similar to the *H* center widely studied in alkali halides. Larger aggregates, e.g. I_3^{2-} are energetically possible but less favorable. Interestingly, the calculated formation energy of primary Frenkel pair of the *F* and *H* centers is smaller than the band gap, which alludes to a possible defect formation under visible light illumination. The defect level positions in the gap show that the *F* center is a shallow donor, the self-trapped hole (V_k center) a shallow acceptor, whereas the *H* center produces energy levels close to the middle of the band gap and as such can behave as a deep electron or hole trap.

Acknowledgments

Many thanks to A. Lushchik, A. Popov and R. Merkle for numerous fruitful discussions. This study was partly supported by the Latvian Council for Science (grant LZP-2018/1-0147 to EK). R.A.E acknowledges the assistance of the University Computer Center of Saint-Petersburg State University for high-performance computations.

References

1. Kojima, A., Teshima, K., Shirai, Y. & Miyasaka, T. Organometal Halide Perovskites as Visible-Light Sensitizers for Photovoltaic Cells. *J. Am. Chem. Soc.* **131,** 6050–6051 (2009).

2. Swarnkar, A. *et al.* Quantum dot-induced phase stabilization of -CsPbI3 perovskite for high-efficiency photovoltaics. *Science (80-.).* **354,** 92–95 (2016).

3. Zhao, B. *et al.* Thermodynamically Stable Orthorhombic γ-CsPbI3Thin Films for High-Performance Photovoltaics. *J. Am. Chem. Soc.* **140,** 11716–11725 (2018).

4. Eperon, G. E. *et al.* Inorganic caesium lead iodide perovskite solar cells. *J. Mater. Chem. A* **3,** 19688–19695 (2015).

5. Huang, Y., Yin, W.-J. & He, Y. Intrinsic Point Defects in Inorganic Cesium Lead Iodide Perovskite CsPbI3. *J. Phys. Chem. C* **122,** 1345–1350 (2018).

6. Li, Y. *et al.* Intrinsic point defects in inorganic perovskite CsPbI3 from first-principles prediction. *Appl. Phys. Lett.* **111,** 162106 (2017).

7. Mizusaki, J., Arai, K. & Fueki, K. Ionic conduction of the perovskite-type halides. *Solid State Ionics* **11,** 203–211 (1983).

8. Yamada, K. *et al.* Phase Transition and Electric Conductivity of ASnCl3 (A = Cs and CH3NH3). *Bull. Chem. Soc. Jpn.* **71,** 127–134 (1998).

9. Yamada, K., Isobe, K., Okuda, T. & Furukawa, Y. Successive Phase Transitions and High Ionic Conductivity of Trichlorogermanate (II) Salts as Studied by 35Cl NQR and Powder X-Ray Diffraction. *Zeitschrift für Naturforsch. A* **49,** 258–266 (1994).

10. Yang, T.-Y., Gregori, G., Pellet, N., Grätzel, M. & Maier, J. The Significance of Ion Conduction in a Hybrid Organic-Inorganic Lead-Iodide-Based Perovskite Photosensitizer. *Angew. Chemie Int. Ed.* **54,** 7905–7910 (2015).

11. Senocrate, A. *et al.* The Nature of Ion Conduction in Methylammonium Lead Iodide: A Multimethod Approach. *Angew. Chemie Int. Ed.* **56,** 7755–7759 (2017).

12. Senocrate, A. *et al.* Charge carrier chemistry in methylammonium lead iodide. *Solid State Ionics* **321,** 69–74 (2018).

13. Azpiroz, J. M., Mosconi, E., Bisquert, J. & De Angelis, F. Defect migration in methylammonium lead iodide and its role in perovskite solar cell operation. *Energy Environ. Sci.* **8,** 2118–2127 (2015).

14. Eames, C. *et al.* Ionic transport in hybrid lead iodide perovskite solar cells. *Nat. Commun.* **6,** 7497 (2015).

15. Haruyama, J., Sodeyama, K., Han, L. & Tateyama, Y. First-Principles Study of Ion Diffusion in Perovskite Solar Cell Sensitizers. *J. Am. Chem. Soc.* **137,** 10048–10051 (2015).

16. Yin, W.-J., Shi, T. & Yan, Y. Unusual defect physics in CH3NH3PbI3 perovskite solar cell absorber. *Appl. Phys. Lett.* **104,** 063903 (2014).

17. Walsh, A., Scanlon, D. O., Chen, S., Gong, X. G. & Wei, S.-H. Self-Regulation Mechanism for Charged Point Defects in Hybrid Halide Perovskites. *Angew. Chemie Int. Ed.* **54,** 1791–1794 (2015).

18. Du, M. H. Efficient carrier transport in halide perovskites: theoretical perspectives. *J. Mater. Chem. A* **2,** 9091–9098 (2014).

19. Whalley, L. D., Crespo-Otero, R. & Walsh, A. H-Center and V-Center Defects in Hybrid Halide Perovskites. *ACS Energy Lett.* 2713–2714 (2017). doi:10.1021/acsenergylett.7b00995

20. Minns, J. L., Zajdel, P., Chernyshov, D., van Beek, W. & Green, M. A. Structure and interstitial iodide migration in hybrid perovskite methylammonium lead iodide. *Nat. Commun.* **8,** 15152 (2017).

21. Peng, C., Wang, J., Wang, H. & Hu, P. Unique Trapped Dimer State of the Photogenerated Hole in Hybrid Orthorhombic CH3NH3PbI3 Perovskite: Identification, Origin, and Implications. *Nano Lett.* **17,** 7724–7730 (2017).

22. Meggiolaro, D., Mosconi, E. & De Angelis, F. Modeling the Interaction of Molecular Iodine with MAPbI3: A Probe of Lead-Halide Perovskites Defect Chemistry. *ACS Energy Lett.* **3,** 447–451 (2018).

23. Kim, G. Y. *et al.* Large tunable photoeffect on ion conduction in halide perovskites and implications for photodecomposition. *Nat. Mater.* **17,** 445–449 (2018).

24. *Point Defects in Solids*. (Springer US, 1972). doi:10.1007/978-1-4684-2970-1

25. Stoneham, A. M. *Theory of Defects in Solids*. (Oxford University Press, 2001). doi:10.1093/acprof:oso/9780198507802.001.0001

26. Kotomin, E. A. & Popov, A. I. Radiation-induced point defects in simple oxides. *Nucl. Instruments Methods Phys. Res. Sect. B Beam Interact. with Mater. Atoms* **141,** 1–15 (1998).

27. Lushchik, A., Kirm, M., Lushchik, C. & Vasil'chenko, E. Excitonic and electron–hole mechanisms of the creation of Frenkel defect in alkali halides. *Nucl. Instruments Methods Phys. Res. Sect. B Beam Interact. with Mater. Atoms* **166–167,** 529–537 (2000).

28. Williams, R. T. & Song, K. S. The self-trapped exciton. *J. Phys. Chem. Solids* **51,** 679–716 (1990).

29. Song, K. S. & Williams, R. T. *Self-Trapped Excitons*. **105,** (Springer Berlin Heidelberg,

1993).

30. Popov, A. I., Kotomin, E. A. & Maier, J. Analysis of self-trapped hole mobility in alkali halides and metal halides. *Solid State Ionics* **302,** 3–6 (2017).

31. Lushchik, A., Lushchik, C., Vasil'chenko, E. & Popov, A. I. Radiation creation of cation defects in alkali halide crystals: Review and today's concept (Review Article). *Low Temp. Phys.* **44,** 269–277 (2018).

32. Brudevoll, T. & Kotomin, E. Interstitial-oxygen-atom diffusion in MgO. *Phys. Rev. B - Condens. Matter Mater. Phys.* **53,** 7731–7735 (1996).

33. Lushchik, A. *et al.* Dependence of long-lived defect creation on excitation density in MgO single crystals. *Phys. status solidi* **4,** 1084–1087 (2007).

34. Seeman, V., Reifman, S., Lehto, T. & Haldre, Ü. Family of O Centres in SrO Crystals. *Phys. status solidi* **102,** 459–465

35. Zhukovskii, Y. F., Platonenko, A., Piskunov, S. & Kotomin, E. A. Ab initio simulations on migration paths of interstitial oxygen in corundum. *Nucl. Instruments Methods Phys. Res. Sect. B Beam Interact. with Mater. Atoms* **374,** 29–34 (2016).

36. Evarestov, R. A., Platonenko, A., Gryaznov, D., Zhukovskii, Y. F. & Kotomin, E. A. First-principles calculations of oxygen interstitials in corundum: a site symmetry approach. *Phys. Chem. Chem. Phys.* **19,** 25245–25251 (2017).

37. Dovesi, R. *et al.* CRYSTAL17 User's Manual. (2017). Available at: http://www.crystal.unito.it/Manuals/crystal17.pdf.

38. Perdew, J. P. *et al.* Restoring the Density-Gradient Expansion for Exchange in Solids and Surfaces. *Phys. Rev. Lett.* **100,** 136406 (2008).

39. CRYSTAL17 Basis Set. Available at: http://crystal.unito.it.

40. Monkhorst, H. J. & Pack, J. D. Special points for Brillouin-zone integrations. *Phys. Rev. B* **13,** 5188–5192 (1976).

41. Evarestov, R. A., Bandura, A. V & Tupitsyn, I. I. Supercell-zone folding transformation for bulk crystals and nanotubes. *Theor. Chem. Acc.* **137,** 14 (2018).

42. Møller, C. K. Crystal Structure and Photoconductivity of Cæsium Plumbohalides. *Nature* **182,** 1436–1436 (1958).

43. Beal, R. E. *et al.* Cesium Lead Halide Perovskites with Improved Stability for Tandem Solar Cells. *J. Phys. Chem. Lett.* **7,** 746–751 (2016).

44. Sharma, S., Weiden, N. & Weiss, A. Phase Diagrams of Quasibinary Systems of the Type: ABX 3 — A′BX 3 ; ABX 3 — AB′X 3 , and ABX 3 — ABX′ 3 ; X = Halogen. *Zeitschrift für Phys. Chemie* **175,** 63–80 (1992).

45. Chen, E. C. M. & Wentworth, W. E. Negative ion states of the halogens. *J. Phys. Chem.*

89, 4099–4105 (1985).

46. Centoni, S. A. *et al*. First-principles calculation of intrinsic defect formation volumes in silicon. *Phys. Rev. B* **72,** 195206 (2005).

47. Alexandrov, V. E., Kotomin, E. A., Maier, J. & Evarestov, R. A. First-principles study of bulk and surface oxygen vacancies in SrTiO3 crystal. *Eur. Phys. J. B* **72,** 53–57 (2009).

Institute of Solid State Physics, University of Latvia as the Center of Excellence has received funding from the European Union's Horizon 2020 Framework Programme H2020-WIDESPREAD-01-2016-2017-TeamingPhase2 under grant agreement No. 739508, project CAMART²